Structured Texture Detection through Fuzzy Texture Spectrum Analysis

M. Grau-Sánchez
Dept. Matemàtica Aplicada II
Univ. Polit. de Catalunya
Barcelona (Spain)
miquel.grau@upc.edu

P. Sobrevilla
Dept. Matemàtica Aplicada II
Univ. Polit. de Catalunya
Barcelona (Spain)
pilar.sobrevilla@upc.edu

E. Montseny
Dept. ESAII
Univ. Polit. de Catalunya
Barcelona (Spain)
eduard.montseny@upc.edu

Abstract

In this paper we present our ongoing work for getting the discrimination power of the Fuzzy Texture Spectrum encoding. The model we propose provides the classes encoded by the spectrum having outstanding power for getting homogeneous, granulated and structured texture image characterization. Moreover, we provide the membership functions allowing getting the degrees to which an image (or image part) is homogeneous, structured and micro-granulated.

Keywords: Texture analysis, Texture Spectrum, Texture characterization, Fuzzy Sets.

1 Introduction

The visual perception of textures has been an area of interest spanning a wide variety of disciplines from art to computer science. The fields of computer vision, perception, and graphics have made significant contributions to the overall understanding of texture perception and representation, although in quite different ways.
From the computer vision point of view, research into texture models ([1, 2]) seeks to find a compact, and if possible complete, representation of textures commonly seen in images. The objective is to use these models for tasks as texture classification, segmenting the parts of an image with different textures, or detecting flaws or anomalies in textures.

The literature distinguishes between stochastic and structural models of texture. A major group of stochastic models is the Probability Density Function (PDF), that model a texture as a random field and a statistical PDF model is fitted to the spatial distribution of intensities in the texture. Typically, these methods measure the interactions of small numbers of pixels.

Probability Density Function methods are divided into parametric and non-parametric. The distinction between both methods reflects the distinction made in statistics between parametric and non-parametric PDF modelling techniques. Examples of non-parametric PDF models are: Gray-Level Co-occurrence Matrices (GLCM), Gray-Level Difference Methods (GLD) and Texture Spectrum Methods. The latest use PDF models that are sensitive to high order interactions.

Texture Spectrum coding (TS) [3], and Local Binary Patterns method (LBP) [4] are the most known non-parametric PDF techniques. From its introduction, these models have been applied for texture analysis classification and characterization, as well as texture-based image segmentation ([3], [5, 6, 7, 8, 9]). Moreover, some authors have explored these methods for developing new texture feature extraction models that allow capturing different aspects of the image texture ([10, 11, 12]). However both methods suffer of some drawbacks. Besides the large range of possible values, another problem of the TS is that, due to the

L. Magdalena, M. Ojeda-Aciego, J.L. Verdegay (eds): Proceedings of IPMU'08, pp. 1183–1190
Torremolinos (Málaga), June 22–27, 2008

way the spectrum is obtained, in natural images it doesn't reflect the human perception of homogeneity. On the other hand, although the LBP reduce the range of possible values, it discards important pattern information (as for homogeneity, due to rules the equality out), and lost the spatial distribution information of the patterns.

Since the upcoming of Soft Computing, intelligent techniques have been introduced to apply the feature classification approach to a growing class of textures [13, 14]. Fuzzy-based methods have been used in texture analysis tasks, particularly for image segmentation, [13]. Some of these methods are based on the TS encoding ([14, 15, 16]), and have been used for texture analysis and classification.

In [17] we introduced the Fuzzy Texture Spectrum (FTS) that, although based on the TS encoding, makes use of the fuzzy techniques to alleviate its drawbacks and problems. Later on, [18], we explored its potential for homogeneous texture characterization proving its superior performance and robustness with regard the TS encoding.
Following our work on the analysis of the FTS coding for extracting texture characterization [19], this work outlines further advances for getting the classes encoded by the Reduced FTS (RFTS) allowing determine the degrees to which the image is homogeneous, granulated and structured.

The paper is structured as follows: Sections 2 and 3 outline the principles of the TS and FTS, as well as the process followed for obtaining the granulated and homogeneous relevant classes and membership functions. Afterwards, the process followed for getting the classes allowing detect the presence of some structure within an image is presented. Section 4 sketch some experimental results. We finish with some Conclusions.

2 Reduced Fuzzy Texture Spectrum

The definition of Texture Spectrum, introduced by He and Wang [3, 5], employs the determination of the Texture Feature Vector (TFV), and the Texture Unit Number (NTFV) values. TFVs characterize the local texture information for a given pixel and its neighbors in a 3x3 window, and the statistics of all the TFVs over the whole image reveal the global texture aspects.
This technique compares the gray-level of the seed pixel, V_0, with those of its neighbors, V_i ($1 \leq i \leq 8$), and records three logical relationships: smaller -0-, equal -1- and greater -2-. So, each image pixel generates an 8-D Texture Feature Vector (E_1, $E_2, \cdots, E_7$, E_8) that can be one of the $3^8 = 6561$ possible vectors. The TFVs have associated Texture Unit Numbers, $N_{TFV} = \sum_{1 \leq i \leq 8} E_i \cdot 3^{i-1}$, that are the labels of the TFVs, and their occurrence frequency function give the Texture Spectrum.

2.1 Fuzzy Texture Spectrum

As in the case of the TS, the start point of the FTS is the set of pixels' intensity values of a 3x3 window centered in the pixel. However, unlike the TS, in the Fuzzy Texture Spectrum encoding (FTS) [17, 18] three values are assigned to a component of the feature vector, each showing the degree to which the gray-levels of surrounding pixels are lighter, μ_0, similar, μ_1, or darker, μ_2 than the central pixel gray-level. So, if $d^i = V_i - V_0$ occupies the same position than pixel i, and $\mu_0^i = \mu_0(d^i)$, $\mu_1^i = \mu_1(d^i)$, $\mu_2^i = \mu_2(d^i)$ are the degrees to which d^i is 0, 1, and 2 respectively, the Fuzzy Texture Feature Vector (FTFV) associated to the seed pixel of the raster window is given by $FTFV = (F_i)_{1 \leq i \leq 8} = ((0_{\mu_0^i}, 1_{\mu_1^i}, 2_{\mu_2^i}))_{1 \leq i \leq 8}$ with $\sum_{j=0,1,2} \mu_1^i = 1$.

So, while the TS assigns a unique Texture Unit Number to the central pixel, the FTS method assigns a set of Fuzzy Texture Unit Numbers, $\{N_{FTFV_k}\}_{k=1}^{l} = \{(N_{TFV_k}, \mu_{N_{TFV_k}})\}_{k=1}^{l}$ which corresponds to the possible combinations obtained from the FTFVs, when $\mu_j^i \neq 0; j = 0, 1, 2$, and their membership degrees are obtained multiplying the corresponding membership degrees.

2.2 Reduced FTS

Although the FTS has proved to reflect texture image characteristics better than the TS

[17, 18], a drawback of both methods is the high number of possible TFVs. Some efforts have been carried out for reducing the complexity of the original TS encoding [20].
In the case of the FTS, we modified its coding scheme grouping in the same class all Texture Feature Vectors differing from rotations multiples of 45 degrees [18]. It allowed reducing spectrum dimensions to 834 *classes* without losing texture characterization power but improving *FTS* efficiency.

3 Granulated and Homogeneous Relevant Classes Detection

Accordingly to human beings inspection, it seems clear that not all the Fuzzy Texture Spectrum Classes (FTSC) are equally significant for texture characterization and discrimination. This why, as a first step, in [19] we developed an heuristic analysis that allowed us to get the classes having outstanding relevance for determining the degree to which an image part is granulated and homogeneous. To do it, starting from a 512x512 homogeneous synthetic image of grey-level equal to 128, H_0, we corrupted it with white noise of sigma values varying from 1 to 15, with gaps of two units (Fig.1), $H_\sigma, \sigma = 1+2k, 1 \leq k \leq 7$, till getting a fine-grained-tipped image, H_{15}.

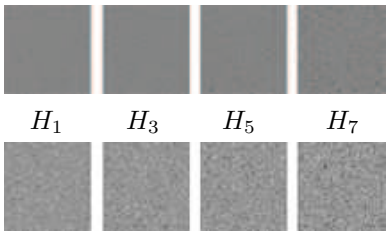

Figure 1: Images considered for obtaining the *Fuzzy Texture Spectrum Classes* having Granulated/Homogeneous discrimination degree.

Then, we analyzed the spectrums obtained using the membership functions of equations (2), (1), and (3), for detecting the classes providing granulated and homogeneous texture information, as well as the degree to which a given image is granulated and homogeneous.

$$\mu_1(d^i) = \begin{cases} 0 & \text{if} \quad \mid d^i \mid \geq 8 \\ \frac{8 - \mid d^i \mid}{5} & \text{if} \quad 3 < \mid d^i \mid < 8 \\ 1 & \text{if} \quad \mid d^i \mid \leq 8 \end{cases} \quad (1)$$

$$\mu_0(d^i) = \begin{cases} 0 & \text{if} \quad d^i \geq 0 \\ 1 - \mu_1(d^i) & \text{if} \quad d^i < 0 \end{cases} \quad (2)$$

$$\mu_2(d^i) = \begin{cases} 0 & \text{if} \quad d^i \leq 0 \\ 1 - \mu_1(d^i) & \text{if} \quad d^i > 0 \end{cases} \quad (3)$$

After detecting the classes accomplishing aforementioned condition, and considering that images go from super-homogeneous, H_1, to granulated, H_{15}, we grouped in the same *over-class* the classes behaving equal for all images. This way we found four *over-classes*: $O_7 = \left\{\overline{01111111}, \overline{11111112}\right\}$, $O_8 = \left\{\overline{11111111}\right\}$, $Z_8 = \left\{\overline{00000000}, \overline{22222222}\right\}$, and $Z_7 = \left\{\overline{00000001}, \overline{12222222}\right\}$.

3.1 Defining Granulated and Homogeneous Membership Functions

Taking into consideration the appearance of the "*relevant classes*" within the synthetic images we obtained the membership functions allowing to get the degrees to which an image (or image region) is Granulated, μ_G, and Homogeneous, μ_H. Noting by $f_{O_7}, f_{O_8}, f_{Z_7}$, and f_{Z_8} the frequencies of appearance of the corresponding *over-classes*, if N is the images size, the membership functions were defined by:

$$\mu_G = max\left\{0, min\left\{1, \frac{1}{2} - 2 \cdot o + 2 \cdot z\right\}\right\} \quad (4)$$

$$\mu_H = max\left\{0, min\left\{1, \frac{1}{2}(1 + o - z)\right\}\right\} \quad (5)$$

where $o = \frac{f_{O_7} + f_{O_8}}{N}$ and $z = \frac{f_{Z_7} + f_{Z_8}}{N}$.

The results obtained by the set of synthetic images were validated considering two additional sets of images obtained in the same way, but starting from synthetic images of grey-levels equal to 60 and 200 respectively. Furthermore, using discriminatory and entropy measures, it was proved the robustness of the FTS for describing homogeneous textures as well as its superior performance with regard the original encoding.

4 Structured Classes Obtaining

In accordance with Haralick [1], besides homogeneous and granulated, image texture can

be qualitatively evaluated as having other properties that depend on tonal primitives and spatial interaction between them, and that we can group within a unique named Structured according to next definition.

Definition. *An image part presents some kind of Structure if within it appears a uniform/repetitive pattern (object), as a geometric shape, or something irregular, but in a repetitive way, as stones or any kind of natural object.*

So, due to the FTSCs are obtained considering not only pixels grey-levels, but also their relative variations within the surroundings, it seems clear that only considering some Classes it would be enough to provide information, at some degree, of the presence of Structure, as it happens for Homogeneous and Granulated properties.

4.1 Classes Identification

The FTSCs having outstanding relevance for determining the degree to which an image part has some kind of macro-texture or Structure have been obtained through a three-steps process based on the analysis of structured synthetic images.

4.1.1 First Step

This step is divided into two parts: *A.- Structured synthetic images design*, and *B.- Obtainment of the images'* FTSs, *and Relevant classes detection.*

A.- Structured synthetic images design. For getting the set of training synthetic images OI=$\{C, T, B, R\}$ we drawn four A4 Word documents made up by homogeneously distributed basic structures: one with 12 circles, C, other with 15 equilateral triangles, T, and the others with 6 bands, B, and 9 rectangles, R, respectively (Fig. 2).

Then, after reducing grey-levels differences between background and objets, we printed the documents and scanned in them at different orientations, except for the circles, and at two resolutions (pixels/cm): l and h. Specifically, bands and rectangles were scanned in

Figure 2: Original synthetic images OI=$\{C, T, B, R\}$ used for obtaining the structured relevant Classes

at 0, 10, 30, 60, and 90 degrees; and triangles at 0, 10, 30, and 60 degrees. On the other hand, for example, circles dimensions at resolutions l and h were of 60x60 and 130x130 pixels, respectively.

Finally, as we were interested in considering structure and images' spectrum modifications on account of noise, we processed previous images adding white noise of sigma values 1, 3, and 12, so obtaining 90 images.

B.- Obtainment of the images' RFTSs and Relevant classes detection. After obtaining the reduced FTSs of previous images we analyzed them looking for the prominent structured *over-classes*. This analysis was based on the comparison of the spectrums obtained for the training images with those of the image H_0 to which we added the same noise level. i.e. if $C_{(r,o,\sigma)}$ notes the image of circles, scanned in at resolution r and orientation o, and processed adding σ white noise, we compared its FTS with that of H_σ.

Finally we got the set of classes expressed in the RFTSs of the training images I_1= $\{C_{(r,o,i)}, T_{(r,o,i)}, B_{(r,o,i)}, R_{(r,o,i)}\}$; r=l, h; o=0, 10, 30, 60, 90; i=1, 3, 12; with frequencies higher than in those of the H_i.

4.1.2 Second Step

Considering that in a Structured image the repetitive patterns can appear with different densities, we designed a second training set of synthetic images, $3OI_d$=$\{3C_d, 3T_d, 3B_d, 3R_d\}$, based on OI but with greater density of elements. To do it, after drawing the set of images OI_d=$\{C_d, T_d, B_d, R_d\}$ (see Fig. $3-a$), each obtained from the corresponding image of OI reducing the space among objects proportionally to their dimensions, we put together three of these images to form the images of $3OI_d$.

Table 1: Classes having outstanding relevance for getting the degrees to which an image is Homogeneous, Structured and Granulated.

Homogeneous	$O_8 = \{\overline{11111111}\}$; $O_7 = \{\overline{01111111}, \overline{11111112}\}$;
Structured	$O_5 = \{\overline{00011111}, \overline{11111222}\}$; $Z_5 = \{\overline{00000222}, \overline{00022222}\}$;
	$O_4 = \{\overline{00011121}, \overline{00011211}, \overline{00012111}, \overline{01222111}, \overline{01122211}, \overline{01112221}\}$;
	$O_3 = \{\overline{00011221}, \overline{00012211}, \overline{00122211}, \overline{00112221}\}$; $O_2 = \{\overline{00012221}\}$;
	$O_1 = \{\overline{00001222}, \overline{00002221}, \overline{00022221}, \overline{00012222}\}$; $Z_4 = \{\overline{00002222}\}$
Granulated	$Z_8 = \{\overline{00000000}, \overline{22222222}\}$; $Z_7 = \{\overline{00000001}, \overline{12222222}\}$

Figure 3 $-b$ depicts the case of image $3C_d$, rotated 90 degrees.

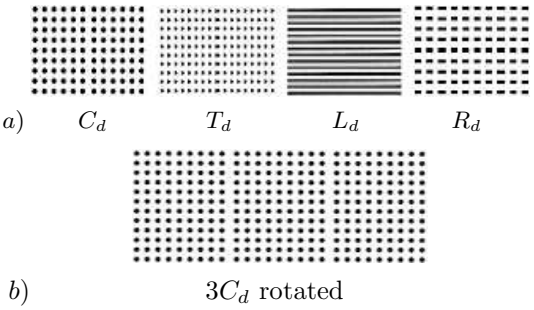

Figure 3: Original synthetic images OI_d=$\{C_d, T_d, L_d, R_d\}$ used for obtaining the structured relevant Classes

Then, starting from $3OI_d$, the process carried out for getting the new training set, and detecting the *Relevant classes*, was the same as at first step, but scanning the A4 documents in at three different resolutions, l, h, and vh, given a total of 135 training images I_2= $\{C_{d_{(r,o,i)}}, T_{d_{(r,o,i)}}, B_{d_{(r,o,i)}}, R_{d_{(r,o,i)}}\}$; $r = l, h, vh$; o=0, 10, 30, 60, 90; i=1, 3, 12. As a consequence of this step, besides confirming the relevance of the classes detected at first step, we made a first approach to the way those classes might be considered for getting the degrees to which an image part is *Homogeneous*, *Granulated* and *Structured*.

4.1.3 Third Step

With the aim of obtaining more intermediate data we processed the images obtained at previous step at noise levels of σ values 6 and 24; I_3= $\{C_{d_{(r,o,i)}}, T_{d_{(r,o,i)}}, B_{d_{(r,o,i)}}, R_{d_{(r,o,i)}}\}$; $r = l, h, vh$; o=0, 10, 30, 60, 90; i=6, 24. The new 90 training images provided us with much more intermediate values and results. Then we obtained the results that are presented at next section.

5 Experimental Results

Table 1 depicts the final set of relevant over classes having outstanding relevance for determining if an image part is Homogeneous, Structured and micro-Granulated at some degree. In order to be minority respectful, classes having equivalent window behavior have been grouped.

5.1 Relevant Classes

Although other classes were also expressed, they wasn't considered because their behavior was equivalent at the synthetic images and at the corresponding H_σ, for the different noise levels. So, in the cases of Homogeneous and micro-Granulated, although other classes were selected at first step, and seemed to be confirmed at second one, were rejected because, at third step, it was proved that the information provided by those classes were the same that the supplied by O_8 and O_7 in the case of Homogeneous, and by Z_8 and Z_7 in the case of micro-Granulated.

For determining the classes having Structured relevance, due to the images we are working with are macro-structured, we selected the classes having clear macro-Structure meaning, and rejected those whose behavior doesn't provide additional relevant information. So, we rejected the classes expressed with higher frequencies for images of $I = \{I_1, I_2, I_3\}$ than for those of H_σ, but whose increasing/decreasing behavior was similar.

For each training image we obtained the relative frequencies of the relevant over-classes,

$f_{O_8}, f_{O_7}, f_{Z_5}, f_{Z_4}, f_{O_5}, f_{O_4}, f_{O_3}, f_{O_2}, f_{O_1}, f_{Z_8}$, and f_{Z_7}. After an analysis of these frequencies, for all the images of I, we found that the quantities related to homogeneity, H, Granularity, G, and Structure, S, of an image can be given by:
$H = f_{O_8} + f_{O_7}$, $G = 4 \cdot (f_{Z_8} + f_{Z_7})$, and
$S = f_{Z_5} + f_{Z_4} + f_{O_5} + f_{O_4} + f_{O_3} + f_{O_2} + f_{O_1}$.

For getting the value of G we have multiplied for 4 the value of $G = f_{Z_8} + f_{Z_7}$ because, in the case of $\sigma = 24$ for which the image H_σ is granulated, that value only arrives to 24.674.

Table 2 depicts the values obtained for the image of triangles scanned at low resolution, for different noise levels, and the corresponding frequencies for images H_σ.
As it was expected, with noise $\sigma = 24$ the classes expressed are mainly Z_8 and Z_7, what means that images are basically micro-Granulated, while for noise $\sigma = 1$ the expressed classes are associated to Homogeneity and to the Structure marked by the frontier among elements and background. Having a look at the values of Structure, row thirteenth (S), it can be appreciated that, for $3 \leq \sigma \leq 12$, this quantity is around a 25% smaller for the H_σ than for the synthetic Structured images. Similar results have been obtained for all the images of I.
It has been also observed that Structured images constituted by small objects are less detected than if are constituted by big objects, except in the cases of high density.

5.2 Membership Functions Obtaining

For obtaining the membership functions we have analyzed the influence of noise and resolution changes within the values of H, S, and G obtained for the images of I. As an example, table 3 depicts the results obtained in the case of the images of triangles scanned at 0 (col. 2 and 3), 30 (col. 4 and 5), and 60 (col. 6 and 7) degrees, for resolutions h (col. 2, 4, 6) and l (col. 3, 5, 7), and noise levels 1 (rows 2-4), 3 (rows 6-8), 6 (rows 10-12), 12 (rows 14-16), and 24 (rows 18-20).

Having a look at table 3 can be appreciated that, except for the case of G, the values obtained are greater for high (col. 2, 4, and 6) than for low resolution (col. 3, 5, and 7). Besides, this characteristic is strongest for low sigma values than for high ones. The case of resolution vh doesn't appear at the table because the values are very similar to the obtained for resolution h.

Looking at the values of H and G, it can be appreciated that, they vary within different ranges for different σ values. So, given the values of H and G for a given image, it is possible to deduce the noise-level of such image. This fact must be considered for defining the membership functions.

Making a comparative study of the tables obtained for all the images of I, we have observed that:

- Structure is better detected if it is constituted by big elements, except if there is high density.
- Membership functions must boost S when H is high.
- Values of S within [0, 2.25], are noisy generated, but out of this interval the value of S begins to be real.

From previous conditions, and analyzing the results for the synthetic images, we constructed three linear functions η_H, η_S, and η_G going through the points $(x, \eta_H(x))$, $(x, \eta_S(x))$, and $(x, \eta_G(x))$ of table 4.

Table 4: Points considered for obtaining lineal functions approaching the membership functions

H	S	G	$\eta_*(X)$, X=H, S, G
0	0	0	0
0.05	2.25	0.08	0.2
10	10	45	0.4
50	17	64	0.6
85	60	88	0.8
100	100	100	1

Then, the membership functions were obtained approaching functions η_H, η_S, and η_G by parabolic functions that minimize the minimum quadratic error, what provided the membership functions:
$\mu_H(x) = 0.0640 + 0.0165 \cdot x - 0.00007127 \cdot x^2$
$\mu_S(x) = 0.1579 + 0.0182 \cdot x - 0.00009768 \cdot x^2$
$\mu_G(x) = 0.1021 + 0.0055 \cdot x + 0.00003753 \cdot x^2$

Table 2: Frequencies of appearance of classes of Table 1 for images $\mathbf{T}_{(l,\mathbf{0},\sigma)}$, and its comparison with the frequencies for images H_σ.

Freq.	$\mathbf{T}_{(l,\mathbf{0},\mathbf{1})}$	$\mathbf{H_1}$	$\mathbf{T}_{(l,\mathbf{0},\mathbf{3})}$	$\mathbf{H_3}$	$\mathbf{T}_{(l,\mathbf{0},\mathbf{6})}$	$\mathbf{H_6}$	$\mathbf{T}_{(l,\mathbf{0},\mathbf{12})}$	$\mathbf{H_{12}}$	$\mathbf{T}_{(l,\mathbf{0},\mathbf{24})}$	$\mathbf{H_{24}}$
$\mathbf{f_{O_8}}$	70.315	52.493	16.45	20.431	0.715	0.89	0.006	0.009	0	0
$\mathbf{f_{O_7}}$	10.036	28.567	24,054	27.968	4.032	4.839	0.118	0.129	0.001	0.003
H	*8*0.351	*8*1.060	*4*0.504	*4*8.399	*4.*747	*5.*729	*0.*124	*0.*138	*0.*001	*0.*003
μ_H	**0.930**	**0.933**	**0.615**	**0.696**	**0.141**	**0.156**	**0.066**	**0.066**	**0.064**	**0.064**
$\mathbf{f_{O_5}}$	3.033	0.628	2.712	1.644	1.437	1.431	0.205	0.218	0.018	0.012
$\mathbf{f_{O_4}}$	0.498	0.001	0.663	0.053	0.868	0.62	0.404	0.401	0.051	0.067
$\mathbf{f_{O_3}}$	0.219	0	0.233	0.001	0.278	0.083	0.226	0.188	0.058	0.082
$\mathbf{f_{O_2}}$	1.306	0	0.867	0	0.455	0.006	0.201	0.04	0.057	0.04
$\mathbf{f_{O_1}}$	1.595	0	1.853	0	1.909	0.007	1.588	0.183	0.89	0.464
$\mathbf{f_{Z_5}}$	0.366	0	0.564	0	1.048	0.003	1.734	0.111	2.03	0.662
$\mathbf{f_{Z_4}}$	2.411	0	2.341	0	2.117	0.001	1.672	0.04	1.059	0.25
S	**9.428**	**0.629**	**9.233**	**1.698**	**8.112**	**2.151**	**6.03**	**1.181**	**4.163**	**1.577**
μ_S	**0.321**	**0.169**	**0.318**	**0.188**	**0.299**	**0.197**	**0.264**	**0.179**	**0.232**	**0.186**
$\mathbf{f_{Z_8}}$	0.052	0.032	0.508	0.531	3.859	4.166	9.689	10.375	12.695	15.547
$\mathbf{f_{Z_7}}$	0.135	0.128	1.273	1.321	6.13	6.605	9.51	10.499	11.361	9.127
$\mathbf{f_{Z_7}+f_{Z_8}}$	**0.187**	**0.160**	**1.781**	**1.852**	**9.989**	**10.771**	**20.199**	**20.874**	**24.056**	**24.674**
G	**0.748**	**0.64**	**7.124**	**7.408**	**39.956**	**43.084**	**80.796**	**83.496**	**96.224**	**98.696**
μ_G	**0.106**	**0.106**	**0.147**	**0.145**	**0.382**	**0.409**	**0.791**	**0.823**	**0.979**	**1**

Rows 5, 14, and 18 of table 2 show the Homogeneous, Structured and micro-Granulated membership values for images $\mathbf{T}_{(\mathbf{l},\mathbf{0},\sigma)}$ and H_σ obtained using previous membership functions.

6 Conclusions

From the results presented at previous section it can be observed that it is no necessary analyze the whole Spectrum for homogeneous, granulated and structured texture image characterization, but just the information provided by 27 Texture Numbers is enough for getting useful information. The next step, that is our current work, consists in applying this study to real images for getting their homogeneous, structured and micro-granulated texture information.

Acknowledgements

This work has been partially supported by Spanish CICYT Projects TIC2006-15518, and TIN2007-68063.

References

[1] R.M. Haralick. Statistical and structural approaches to texture. *IEEE TPAMI*, vol.67, pp.786-804, 1979.

[2] M. Tuceryan and A.K. Jain. Texture analysis. In *The handbook of pattern recognition and computer vision*, 2nd ed., World Scientific, pp.207-248, 1998.

[3] D.C. He and L. Wang. Texture unit, texture spectrum and texture analysis. *IEEE Trans. on Geoscience and Remote Sensing*, 28(4), pp.509-512, 1990.

[4] T. Ojala, M. Pietikäinen and D. Harwood. A comparative study of texture measures with classification based on feature distributions. *Pattern Recognition*, vol.29(1), pp.51-59, 1996.

[5] L. Wang and D.C. He. Texture classification using texture spectrum. *Pattern Recognition*, vol. 23(8), pp.905-910, 1990.

[6] D.C. He and L. Wang. Texture features based on texture spectrum. *Pattern Recognition*, vol. 25(3), pp. 391-399, 1991.

[7] T. Mäenpä, T. Ojala, M. Pietikäinen and M. Soriano. Robust Texture Classification by Subsets of Local Binary Patterns. *Proc. 15th Intl Conf. Pattern Recognition* vol.3, pp.947-950, 2000.

[8] C.C. Hung, M. Pham, S. Arasteh, B.C. Kuo and T. Coleman. Image Texture Classification Using Texture Spectrum and Local Binary Pattern. *IEEE Conf. on Geoscience and*

Table 3: Values of H, S, and G obtained for the images of triangles scanned at 0, 30, and 60 degrees; at resolutions h and l ; and with noise of sigma values 1, 3, 6, 12, and 24.

	$\mathbf{T_{(h,0,1)}}$	$\mathbf{T_{(l,0,1)}}$	$\mathbf{T_{(h,30,1)}}$	$\mathbf{T_{(l,30,1)}}$	$\mathbf{T_{(h,60,1)}}$	$\mathbf{T_{(l,60,1)}}$	$\mathbf{H_1}$
H	83.921	80.252	85.456	80.138	84.229	79.17	81.059
S	3.929	2.725	3.524	3.055	3.644	2.623	0.629
G	1.904	6.424	1.12	4.892	1.44	6.092	0.64
	$\mathbf{T_{(h,0,3)}}$	$\mathbf{T_{(l,0,3)}}$	$\mathbf{T_{(h,30,3)}}$	$\mathbf{T_{(l,30,3)}}$	$\mathbf{T_{(h,60,3)}}$	$\mathbf{T_{(l,60,3)}}$	$\mathbf{H_3}$
H	40.903	39.615	41.5786	39.238	40.938	38.545	48.398
S	4.954	3.667	4.905	4.153	5.025	3.792	1.697
G	8.8	13.304	7.756	12	8.124	13.04	7.408
	$\mathbf{T_{(h,0,6)}}$	$\mathbf{T_{(l,0,6)}}$	$\mathbf{T_{(h,30,6)}}$	$\mathbf{T_{(l,30,6)}}$	$\mathbf{T_{(h,60,6)}}$	$\mathbf{T_{(l,60,6)}}$	$\mathbf{H_6}$
H	4.926	4.797	4.965	4.697	4.885	4.691	5.729
S	4.28	3.421	4.378	4.045	4.408	3.64	2.15
G	42.728	45.860	41.584	44.328	41.980	44.932	43.084
	$\mathbf{T_{(h,0,12)}}$	$\mathbf{T_{(l,0,12)}}$	$\mathbf{T_{(h,30,12)}}$	$\mathbf{T_{(l,30,12)}}$	$\mathbf{T_{(h,60,12)}}$	$\mathbf{T_{(l,60,12)}}$	$\mathbf{H_{12}}$
H	0.121	0.113	0.115	0.112	0.121	0.13	0.138
S	2.693	2.241	2.725	2.705	2.725	2.466	1.182
G	80.912	82.048	80.1	80.728	80.348	81.656	83.496
	$\mathbf{T_{(h,0,24)}}$	$\mathbf{T_{(l,0,24)}}$	$\mathbf{T_{(h,30,24)}}$	$\mathbf{T_{(l,30,24)}}$	$\mathbf{T_{(h,60,24)}}$	$\mathbf{T_{(l,60,24)}}$	$\mathbf{H_{24}}$
H	0.001	0.002	0.002	0.001	0.001	0.001	0.003
S	2.657	2.474	2.639	2.759	2.675	2.625	1.577
G	98.548	98.832	96.084	98.348	98.296	98.608	98.696

Remote Sensing (IGARSS 2006), pp.2750-2753, 2006.

[9] N.N. Kachouie and P. Fieguth. A Medical Texture Local Binary Pattern For TRUS Prostate Segmentation. *IEEE Conf. on Engineering in Medicine and Biology Society*, pp.5605-5608, 2007.

[10] K. Jalaja, C. Bhagvati, B. L. Deekshatulu and A.K. Pujari. Texture element feature characterizations for CBIR. *IEEE Intl. Geoscience and Remote Sensing Symposium*, vol.2, pp.733-736, 2005.

[11] T. Ojala, M. Pietikäinen and T. Mäenpää. Multiresolution gray-scale and rotation invariant texture classification with local binary patterns. *IEEE Trans. on Pattern Analysis and Machine Intelligence*, vol.24(7), pp.971-987, 2002.

[12] L. Shu and A.C.S. Chung. Texture Classification by using Advanced Local Binary Patterns and Spatial Distribution of Dominant Patterns. *IEEE Intl. Conf. on Acoustics, Speech and Signal Processing*, vol.1, pp.1221-1224, 2007.

[13] G. Karmakar, L. Dooley and M. Murshed. Fuzzy rule for image segmentation incorporating texture features. *Proc. Int. Conf. on Image Processing*, vol.1, pp.77-80, 2002.

[14] J. S. Taur and C.W. Tao. Texture classification using a fuzzy texture spectrum and neural networks. *Journal of Electronic Imaging*, vol.7(1), pp. 29-35, 1998.

[15] Y.G. Lee, J.H. Lee and Y.C Hsueh. Texture classification using fuzzy uncertainty texture spectrum. *Neurocomputing*, vol.20(1), pp.115-122, 1998.

[16] J.S. Taur, G.H. Lee, C.W. Tao, C.C. Chen and C.W. Yang. Segmentation of psoriasis vulgaris images using multiresolution-based orthogonal subspace techniques. *IEEE Trans. on Systems, Man and Cybernetics, Part B*, vol.36(2), pp.390-402, 2006.

[17] A. Barceló, E. Montseny and P. Sobrevilla. Fuzzy texture unit and fuzzy texture spectrum for texture characterization. *Fuzzy Sets and Systems*, vol. 158(3), pp.239-252, 2007.

[18] A. Barceló, P. Sobrevilla and E. Montseny. Robustness and performance evaluation of the fuzzy texture spectrum encoding. *IEEE World Congress on Comput. Intelligence*, pp.1279-1286, 2006.

[19] M. Grau-Sánchez, E. Montseny, and P. Sobrevilla. On the Use of Fuzzy Texture Spectrum for Homogeneous and Textured Images Discrimination. *IEEE Intl. Conf. on Fuzzy Systems*, pp.1-6, 2007.

[20] B. Xu, P. Gong, R. Seto and R. Spear. Comparison of gray level reduction schemes with a revised texture spectrum method for land-use classification using IKONOS imagery. *Photogrammetric Engineering and Remote Sensing*, vol.69(5), pp.529-536, 2003.